A mitotic nuclear envelope tether for Gle1 also affects nuclear and nucleolar architecture

Mahesh Chemudupati[a,b], Aysha H. Osmani[b], and Stephen A. Osmani[a,b,*]
[a]Ohio State Biochemistry Program and [b]Department of Molecular Genetics, Ohio State University, Columbus, OH 43210

ABSTRACT During *Aspergillus nidulans* mitosis, peripheral nuclear pore complex (NPC) proteins (Nups) disperse from the core NPC structure. Unexpectedly, one predicted peripheral Nup, Gle1, remains at the mitotic nuclear envelope (NE) via an unknown mechanism. Gle1 affinity purification identified mitotic tether for Gle1 (MtgA), which tethers Gle1 to the NE during mitosis but not during interphase when Gle1 is at NPCs. MtgA is the orthologue of the *Schizosaccharomyces pombe* telomere-anchoring inner nuclear membrane protein Bqt4. Like Bqt4, MtgA has meiotic roles, but it is functionally distinct from Bqt4 because MtgA is not required for tethering telomeres to the NE. Domain analyses showed that MtgA targeting to the NE requires its C-terminal transmembrane domain and a nuclear localization signal. Of importance, MtgA functions beyond Gle1 mitotic targeting and meiosis and affects nuclear and nucleolar architecture when deleted or overexpressed. Deleting MtgA generates small, round nuclei, whereas overexpressing MtgA generates larger nuclei with altered nuclear compartmentalization resulting from NE expansion around the nucleolus. The accumulation of MtgA around the nucleolus promotes a similar accumulation of the endoplasmic reticulum (ER) protein Erg24, reducing its levels in the ER. This study extends the functions of Bqt4-like proteins to include mitotic Gle1 targeting and modulation of nuclear and nucleolar architecture.

Monitoring Editor
Mark J. Solomon
Yale University

Received: Jul 26, 2016
Revised: Sep 6, 2016
Accepted: Sep 8, 2016

INTRODUCTION

The nuclear envelope (NE) separates the nucleus and its DNA from the rest of the cell. The NE consists of two juxtaposed membranes—the inner nuclear membrane (INM) facing the nuclear interior, and the outer nuclear membrane (ONM), which is continuous with the endoplasmic reticulum (ER) and faces the cytoplasm (Hetzer, 2010). Alterations of the NE occur during aging and disease (Wolfner and Wilson, 2001; Worman, 2004; Worman *et al.*, 2010; Webster *et al.*, 2009; Walters *et al.*, 2012; Hatch and Hetzer, 2014). For example, aberrant nuclear morphology is a diagnostic marker for cancerous cells (Zink *et al.*, 2004; Chow *et al.*, 2012). It is not only in disease states that the NE can have abnormal structures. In many cell types in both plants and mammals, the NE can form intranuclear invaginations referred to as the nucleoplasmic reticulum, although the functional significance and etiology of these structures are not understood (Malhas *et al.*, 2011).

The NE is traversed by nuclear pore complexes (NPCs), which form sites where the INM and ONM are fused (Doucet *et al.*, 2010; Fichtman *et al.*, 2010; Talamas and Hetzer, 2011) and provide regulated conduits to allow selective transport of macromolecules in and out of nuclei. They are composed of ~30 different proteins called nucleoporins (Nups), which are present in multiple copies per NPC. The structure of NPCs is conserved and contains a core scaffold embedded in the NE, which surrounds the central channel transport pore. Peripheral Nups are anchored to the core scaffold and extend into the central channel, cytoplasm, or nucleoplasm (D'Angelo and Hetzer, 2008).

During mitosis, the NE undergoes dramatic structural changes (Prunuske and Ullman, 2006; Guttinger *et al.*, 2009), and there is great diversity in how organisms modify the NE to ensure successful

This article was published online ahead of print in MBoC in Press (http://www.molbiolcell.org/cgi/doi/10.1091/mbc.E16-07-0544) on September 14, 2016.

*Address correspondence to: Stephen A. Osmani (osmani.2@osu.edu).

Abbreviations used: BLAST, basic local alignment search tool; BLOSUM, blocks substitution matrix; CR, cherry red; DF, dense fibrillar; DiOC6(3), 3,3′-dihexyloxacarbocyanine; DsRed, discosoma red fluorescent protein; ER, endoplasmic reticulum; FC, fibrillar center; 5-FOA, 5-fluoroorotic acid; GC, granular component; GFP, green fluorescent protein; INM, inner nuclear membrane; mRNP, messenger ribonucleoprotein particle; NE, nuclear envelope; NLS, nuclear localization sequence; NOR, nucleolar-organizer region; NPC, nuclear pore complex; Nup, nucleoporin; ONM, outer nuclear membrane; rDNA, ribosomal DNA; RFP, red fluorescent protein; SPB, spindle pole body; TM, transmembrane; TMD, transmembrane domain; WT, wild type.

mitosis. Whereas vertebrate cells completely disassemble their NPCs and NE (open mitosis), in some organisms, both NPCs and the NE remain intact (closed mitosis). Between these extremes, the NE remains physically intact in the model filamentous fungus *Aspergillus nidulans,* but NPCs partially disassemble, with 14 of the ~30 Nups dispersing from the core NPC scaffold (partially open mitosis; De Souza *et al.*, 2004; Osmani *et al.*, 2006a; Liu *et al.*, 2009). All 14 of the dispersed Nups are peripheral Nups. However, 1 peripheral Nup, Gle1, unexpectedly remains at the NE and does not disperse from the NE during mitosis (Osmani *et al.*, 2006a; Ukil *et al.*, 2009). Gle1 is a conserved, essential nuclear RNA export factor with additional roles in translation initiation and termination (Bolger *et al.*, 2008). Shuttling of Gle1 between nucleoplasm and cytoplasm is essential for mRNA export in humans (Kendirgi *et al.*, 2003). Gle1 associates with the cytoplasmic filaments of NPCs and aids in the release of messenger ribonucleoprotein particle (mRNP) complexes into the cytoplasm from the nucleus by activating the ATPase and mRNP remodeling activity of the DEAD-box helicase Dbp5 (Rayala *et al.*, 2004; Kendirgi *et al.*, 2005; Folkmann *et al.*, 2011).

In addition to the partial disassembly of its NPCs, the mitotic NE in *A. nidulans* is also dramatically spatially modified. After anaphase, the NE constricts around daughter nuclei on either side of the nucleolus, which becomes positioned between the segregating chromosomes (Ukil *et al.*, 2009). Therefore the NE surrounds three components during anaphase—the central nucleolus and the two forming daughter nuclei. Although all core Nups localize preferentially to the NE around forming daughter nuclei, Gle1 is an exception and locates evenly at the NE around all three of these components during anaphase by an unknown mechanism. The presence of Gle1 at the mitotic NE in *A. nidulans* is therefore intriguing. We report here the requirement for the tail-anchored integral NE protein mitotic tether for Gle1 (MtgA; an orthologue of *Schizosaccharomyces pombe* Bqt4) for targeting Gle1 to the NE specifically during mitosis and maintaining normal nuclear and nucleolar architecture.

RESULTS

MtgA is a conserved protein identified from Gle1 affinity purification

We previously reported that Gle1 remains at the NE during mitosis, whereas all other peripheral Nups disperse from the NE (Osmani *et al.*, 2006a; Ukil *et al.*, 2009). During anaphase, Gle1 locates at the NE around the centrally positioned nucleolus, whereas core Nup proteins do not (Osmani *et al.*, 2006a; Ukil *et al.*, 2009). We thus reasoned that Gle1 remains at the mitotic NE by associating with a NE protein that is not a core Nup. To test this, we performed Gle1 affinity purifications and identified copurifying proteins by mass spectrometry. Gle1 copurified with two peripheral Nups (SonA and Nup42), the *A. nidulans* importin-α (KapA), and AN0162 (Figure 1A). Because SonA-GFP (De Souza *et al.*, 2004) and KapA-CR (Markina-Inarrairaegui *et al.*, 2011) disperse from nuclei during mitosis (Supplemental Figure S1A), they are unlikely to be the mitotic NE tethers for Gle1. Furthermore, although Nup42 was found to partially remain at the mitotic NE, it is not required for Gle1 targeting to the NE during interphase or mitosis (Supplemental Figure S1B). Therefore we focused on the previously uncharacterized Gle1-copurifying protein encoded from the locus AN0162 as a potential mitotic NE tether for Gle1. From >100 protein affinity purifications, including all known NPC proteins in *A. nidulans*, AN0162 copurified only with Gle1, KapA, and SonA (A.H.O., unpublished data). Of importance, AN0162–S-tag copurified Gle1, as well as Nup42, SonA, and KapA (Supplemental Figure S1C). For reasons discussed later, we named this protein MtgA.

A

Protein	Unique peptides/ % mass spec. coverage
Gle1	23/42%
AN0162 (MtgA)	11/43%
Nup42	15/32.5%
SonA	15/30%
KapA	8/19%

B

A. nidulans protein (gene ID)	*S. pombe* ortholog (e-value)	*S. cerevisae* ortholog (e-value)
RgdA (AN3154)	Res1 (2e-72) Res2 (6e-79)	Swi4 (2e-20)
StuA (AN5836)	-	Sok2 (8e-49) PHD1 (3e-48)
AN6715	Cdc10 (3e-38)	Mbp1 (3e-26)
MtgA (AN0162)	Bqt4 (2e-12)	-

C

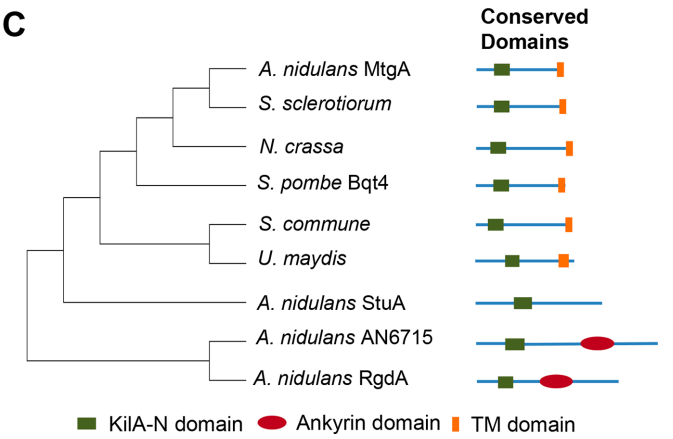

FIGURE 1: MtgA is a transmembrane protein that copurifies with Gle1 and is conserved among the Ascomycetes and Basidiomycetes. (A) Identity and sequence coverage of proteins identified from Gle1–S-tag affinity purification (strain SO901) followed by mass spectrometry. SonA and Nup42 are peripheral Nups. KapA is the orthologue of importin-α. AN0162 (MtgA) is a previously uncharacterized protein with a single-pass TMD at its very C-terminus and a conserved APSES KilA N–like nucleic acid–binding domain (KilA-N). (B) KilA-N proteins in *A. nidulans* and their predicted orthologues in *S. pombe* and *S. cerevisiae*, with *e*-values given in parentheses. (C) Phylogram representing protein orthologues of MtgA across fungi. Organisms shown are *A. nidulans*, *Sclerotinia sclerotiorum* (locus SS1G_08511), *Neurospora crassa* (locus NCU06560), *S. pombe*, *Schizophyllum commune* (locus SCHCODRAFT_269950), and *Ustilago maydis* (locus UMAG_11055). *S. commune* and *U. maydis* are Basidiomycetes. All other taxa are Ascomycetes. StuA, RgdA, and AN6715 are the three other KilA-N proteins in *A. nidulans.*

We were particularly interested in MtgA due to the presence of a single-pass transmembrane domain (TMD) at its very C-terminus (Figure 1A), suggesting that it could integrate into the nuclear membrane. Also of interest was its putative nucleic acid–binding KilA-N domain. The KilA-N–domain family includes the previously defined fungal APSES domain of some fungal transcription factors (Iyer *et al.*, 2002). There are four KilA-N–domain proteins in *A. nidulans*

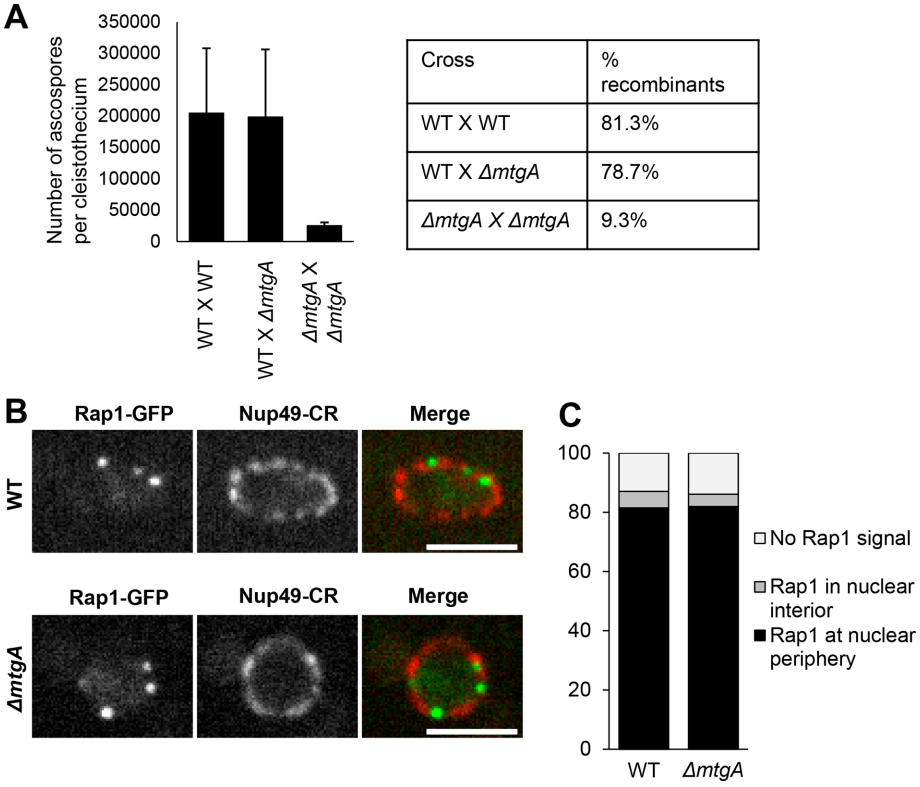

Cross	% recombinants
WT X WT	81.3%
WT X *ΔmtgA*	78.7%
ΔmtgA X ΔmtgA	9.3%

FIGURE 2: Δ*mtgA* strains self-cross poorly but do not display loss of telomere–NE attachment in mitotic cells. (A) Left, ascospores obtained per cleistothecia (average from four cleistothecia) from crossing strains MC112 to SO451 (WT × WT), MC112 to SO1062 (WT × Δ*mtgA*), and MC090 to SO1062 (Δ*mtgA* × Δ*mtgA*). Right, recombination frequencies from 75 progeny from each of the crosses after segregation of markers *pabaA1* (chromosome I), *nimT23* (chromosome II), and *pyroA4* (chromosome IV). (B) Telomere tethering to the NE was unaffected in Δ*mtgA* cells (strain MC261) compared with WT cells (MC240) when observing Rap1-GFP as a telomere marker and Nup49-CR is a marker for the NE. (C) During mitosis, Rap1 disperses throughout cells, and ~80% of nuclei have Rap1-GFP at the nuclear periphery in both WT and Δ*mtgA* cells. The central focal plane was chosen for quantitation in each condition. $n = 114$ for WT and 121 for Δ*mtgA*. Scale bar, 5 μm.

(Figure 1B), but MtgA is the only one with a C-terminal TMD. Phylogenetic analysis revealed that the domain structure of having a KilA-N domain in combination with a single-pass C-terminal TMD is conserved in both the Ascomycetes and Basidiomycetes (Figure 1C). MtgA shares greater sequence homology to its orthologues in other fungi than to the other three KilA-N proteins in *A. nidulans*. Orthologues of MtgA were not identified outside the fungi and are absent in *Saccharomyces cerevisiae* (Figure 1B). The MtgA orthologue in *S. pombe* is Bqt4 (Chikashige *et al.*, 2009), which locates to the INM. Bqt4 mutants that lack the TM domain fail to localize to the INM (Chikashige *et al.*, 2009) but are transported into nuclei.

MtgA is not required for NE telomere attachment during the mitotic cell cycle

In *S. pombe*, Bqt4 is required for formation of the meiotic chromosome bouquet to facilitate efficient chromosome pairing and recombination (Chikashige *et al.*, 2009). Strains that lack *bqt4* cannot cross effectively and display skewed meiotic recombination frequencies and a high degree of ascospore inviability (Chikashige *et al.*, 2009). We therefore deleted *mtgA* and asked whether deleted strains display similar defects. We found *mtgA*-deleted strains had fewer ascospores per cleistothecium (fruiting body) and defects in their meiotic recombination frequency (Figure 2A). The number of ascospores formed per cleistothecium in Δ*mtgA* self-outcrossing strains was reduced by nearly an order of magnitude compared with a wild-type outcross, which is analogous to the effect of Δ*bqt4* on the number of normal four spores formed in *S. pombe* (Chikashige *et al.*, 2009).

Bqt4 tethers telomeres to the NE during the fission yeast mitotic cell cycle and maintains them at the NE during meiosis. In *A. nidulans*, we did not find differences in the localization of the telomere marker Rap1 (AN1906) during the mitotic cell cycle of wild-type cells compared with cells lacking MtgA (Figure 2, B and C). In addition to Bqt4, *S. pombe* has three other proteins involved in bouquet formation: Bqt1, Bqt2, and Bqt3 (Chikashige *et al.*, 2006, 2009). However, none of these is conserved outside the *Schizosaccharomyces* genus. Our data therefore indicate that MtgA is functionally distinct from Bqt4 with regard to telomere tethering to the NE during the mitotic cell cycle, although it is required for normal levels of meiotic recombination.

MtgA is an integral membrane protein of the nuclear envelope

Green fluorescent protein (GFP) fused to the N-terminus of endogenous MtgA localizes to the NE during interphase and mitosis. Of note, just like Gle1-GFP, during mitosis, GFP-MtgA localizes to the NE surrounding the separating daughter nuclei, as well as the centrally positioned nucleolus during telophase (Figure 3A).

Given that MtgA associates with a NPC protein, it could be a transmembrane Nup. We therefore observed GFP-MtgA localization in the *Δnup133* genetic background, which causes NPC clustering (Doye *et al.*, 1994). In this background, proteins associated with NPCs appear in clusters, whereas nuclear membrane proteins adopt a more even distribution around the NE. GFP-MtgA was not seen in NPC clusters (marked by the transmembrane Nup Pom152) and had an even distribution around the NE (100% of 154 nuclei), indicating that it does not associate with NPCs (Figure 3B). This shows that MtgA is a nuclear membrane protein—likely an INM protein like Bqt4 in *S. pombe* (Chikashige *et al.*, 2009).

Some integral INM proteins are transported to the INM after integrating into the endoplasmic reticulum (ER) membrane via their TMD and subsequent nuclear localization sequence (NLS)–dependent transport through the nuclear pore membrane into the INM (King *et al.*, 2006; Lusk *et al.*, 2007; Meinema *et al.*, 2011). Such proteins that lack their NLS but retain their TMD and therefore localize to the ER. To determine whether MtgA localization is consistent with that of an INM protein, we performed a deletion analysis using mCherry-tagged truncated versions of MtgA to replace the wild type and tracked their localization using confocal microscopy (Figure 3C).

To determine whether MtgA requires its TMD for INM insertion, we tested truncations that lacked the TMD or the TMD and

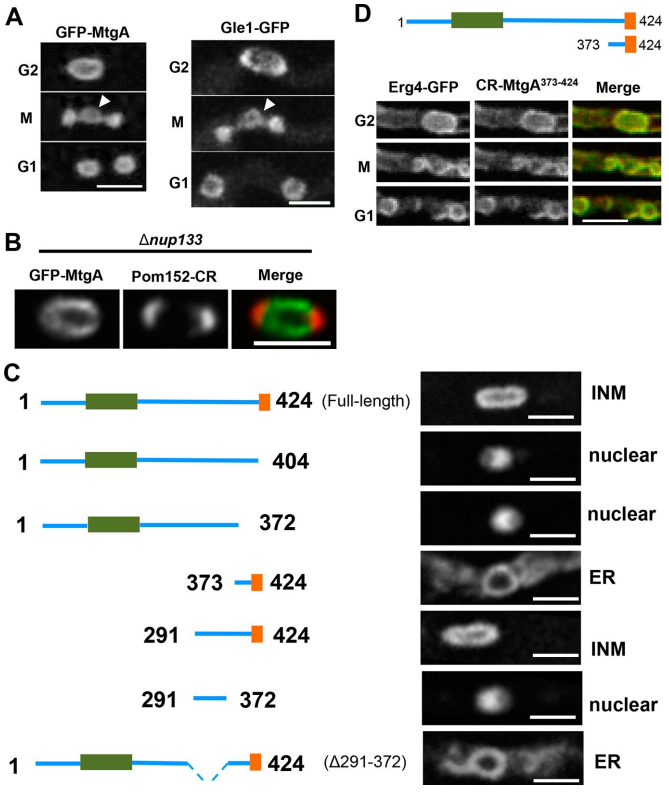

FIGURE 3: MtgA localizes to the NE in a manner that is consistent with an inner nuclear membrane protein. (A) GFP-MtgA (strain MC02) localizes at the NE around the disassembling nucleolus (arrowhead) during mitosis, as does Gle1-GFP (strain MC207). (B) GFP-MtgA does not associate with NPCs, marked by Pom152-CR, in a *Δnup133* background, which causes NPC clustering (strain MC169). (C) Domain analysis of MtgA using endogenously replaced mCherry-tagged truncations as indicated. The TM domain is indicated as the orange C-terminal region, and the KilA-N domain is in green. Representative images of individual locations are also shown. Strains used are MC070 (CR-MtgA), MC117 (CR-MtgA$^{1-404}$), MC174 (CR-MtgA$^{1-372}$), MC116 (CR-MtgA$^{373-424}$), MC115 (CR-MtgA$^{291-424}$), MC212 (CR-MtgA$^{291-372}$), and MC218 (CR-MtgA$^{\Delta 291-372}$). (D) MtgA$^{373-424}$ localizes to the ER, as confirmed by colocalization with the transmembrane ER marker Erg4 (strain MC192). Scale bar, 5 μm.

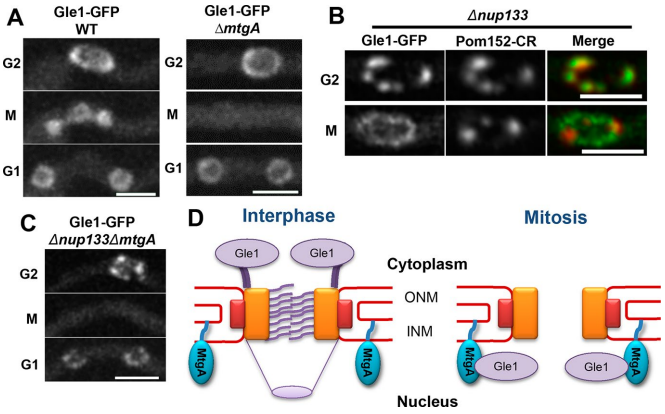

FIGURE 4: Gle1 transfers from NPCs during interphase to the INM via MtgA during mitosis. (A) Gle1-GFP localization in WT (strain MC207) compared with *ΔmtgA* cells (MC206), showing that Gle1 requires MtgA for its mitotic localization. (B) NPC clustering assay with Gle1-GFP in conjunction with Pom152-CR (strain MC157). During interphase, Gle1-GFP associates with NPC clusters marked by Pom152-CR. However, during mitosis (M), Gle1-GFP adopts a smoother NE distribution and does not associate with NPC clusters. (C) Gle1-GFP localizes to NPC clusters during interphase but disperses from the NE in strain MC167, which lacks both *nup133* and *mtgA*. (D) Model for Gle1 localization during interphase and then mitosis. During interphase, Gle1 is at NPCs, but it transitions from NPCs to the INM during mitosis via MtgA. Scale bar, 5 μm.

32 amino acids (aa) N-terminal to it (MtgA$^{1-372}$). Neither was able to integrate into the INM but instead localized to the nuclear interior (in 96.7% of 303 nuclei expressing CR-MtgA$^{1-404}$, and 98% of 603 nuclei expressing CR-MtgA$^{1-372}$), indicating that they contained a functional NLS (Figure 3C, 1–404 and 1–372). Further analysis confirmed that MtgA contains a functional NLS between aa 291 and 372 (Figure 3C, 291–372, 97.6% of 206 nuclei). This version and the version lacking only the TMD both localize exclusively to nuclei during interphase but then disperse from nuclei during mitosis like other nuclear proteins, including NLS-DsRed (De Souza *et al.*, 2004; Supplemental Figure S2). Expressing the TMD with the 32 aa N-terminal to it (373–424) resulted in a protein that localized to the ONM/ER (99.4% of 513 nuclei) colocalizing with the ER marker Erg4 (Figure 3D, 100% of 130 nuclei), whereas addition of aa from 291 (291–424) allowed targeting exclusively to the INM (Figure 3C, 100% of 469 nuclei). Because MtgA requires both its C-terminal TMD and an NLS for localization exclusively to the NE, it behaves like an integral INM protein, like its fission yeast orthologue, Bqt4.

During mitosis, Gle1 translocates from NPCs to MtgA

To test whether MtgA tethers Gle1 to the NE during mitosis, we followed Gle1-GFP distribution during the cell cycle in *ΔmtgA* cells. In contrast to wild-type cells, in which Gle1 remains at the NE during mitosis, in the *ΔmtgA* background, Gle1-GFP locates normally to the NE during interphase but disperses from the NE during mitosis and returns to the NE upon completion of mitosis (Figure 4A, 100% of 71 mitoses). This indicates that Gle1 transitions from NPCs to the nuclear membrane via MtgA at mitosis. Of note, it is difficult to observe transition of Gle1 from NPCs to the mitotic nuclear membrane in WT cells due to the close proximity of NPCs with the nuclear membrane. However, in *Δnup133* cells, which have clustered NPCs, this transition was clear. Gle1 located to the NPC clusters (Figure 4B, G2) during interphase but moved from the NPC clusters onto the nuclear membrane during mitosis (Figure 4B, M; 100% of 84 mitoses). If the transition of Gle1 from NPC clusters to the nuclear membrane during mitosis is via MtgA, then deletion of *mtgA* in the *Δnup133* background would be predicted to result in Gle1 localization to NPC clusters during G2, followed by its dispersal from NPCs into the cytoplasm during mitosis due to the absence of MtgA at the nuclear membrane. Subsequently Gle1 would be expected to return to NPCs after mitotic exit. These expectations are fulfilled in the *Δnup133ΔmtgA* double-deletion background (in 100% of 32 mitoses; Figure 4C). These experiments provide additional lines of evidence that Gle1 associates with NPCs during interphase but dissociates from NPCs during mitosis and localizes to the INM through its association with MtgA. To our knowledge, the data reveal the first instance of a protein targeted to two distinct regions of the NE via different targeting proteins that is regulated in a cell cycle–dependent manner (Figure 4D).

MtgA is required to maintain nuclear shape and size

MtgA-deleted strains have nuclei that are noticeably rounder than wild-type cells (Figure 5A), and their nuclear volume is also reduced

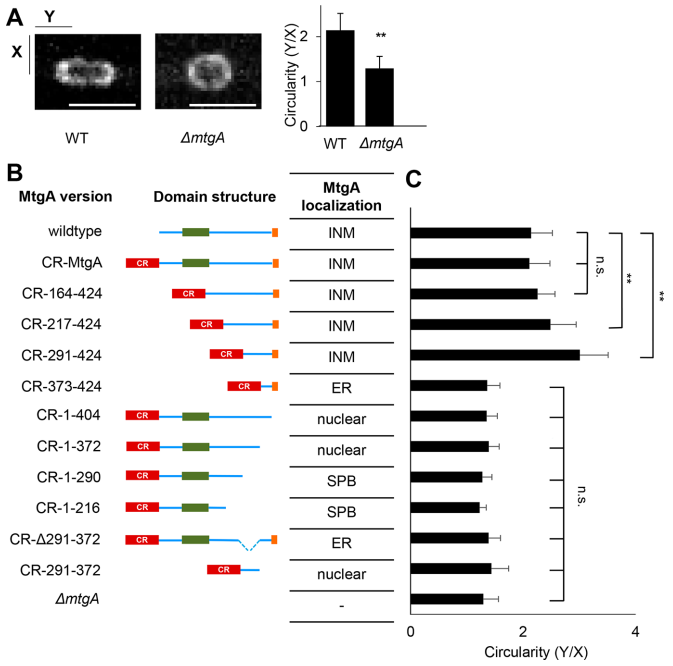

FIGURE 5: MtgA is required for maintaining nuclear morphology. (A) Typical nuclear shape visualized using Gle1-GFP in a WT (strain MC112) vs. Δ*mtgA* strain (MC090), differing only at the *mtgA* locus. Right, circularity (ratio of *Y* to *X*) of WT vs. Δ*mtgA* nuclei ($n = 26$ for WT and 31 for Δ*mtgA*; $^{**}p < 0.01$) (B) Truncated versions of MtgA were generated and expressed from the *mtgA* locus as the sole version of MtgA. The different domain structures are indicated, with the green box indicating the KilA-N domain and the orange box the TMD. Locations were defined using confocal microscopy. The SPB location was only partial, with most of the protein dispersed throughout the cells. (C) Circularity of nuclei (ratio *Y*/*X*) determined by visualizing Gle1-GFP in each of the truncation mutants. $n \geq 25$ for each mutant. Circularities were calculated by measuring Gle1-GFP distribution at the NE for nuclei in late G2, defined as 6–10 min before onset of nuclear division. Strains used are MC206 (WT), MC207 (Δ*mtgA*), MC070 (CR-MtgA), MC111 (CR-MtgA$^{164\text{-}424}$), MC110 (CR-MtgA$^{217\text{-}424}$), MC115 (CR-MtgA$^{291\text{-}424}$), MC116 (CR-MtgA$^{373\text{-}424}$), MC117 (CR-MtgA$^{1\text{-}404}$), MC174 (CR-MtgA$^{1\text{-}372}$), MC155 (CR-MtgA$^{1\text{-}290}$), MC114 (CR-MtgA$^{1\text{-}216}$), MC218 (CR-MtgA$^{\Delta 291\text{-}372}$), and MC212 (CR-MtgA$^{291\text{-}372}$). $^{**}p < 0.01$; n.s., not significant. Scale bar, 5 μm.

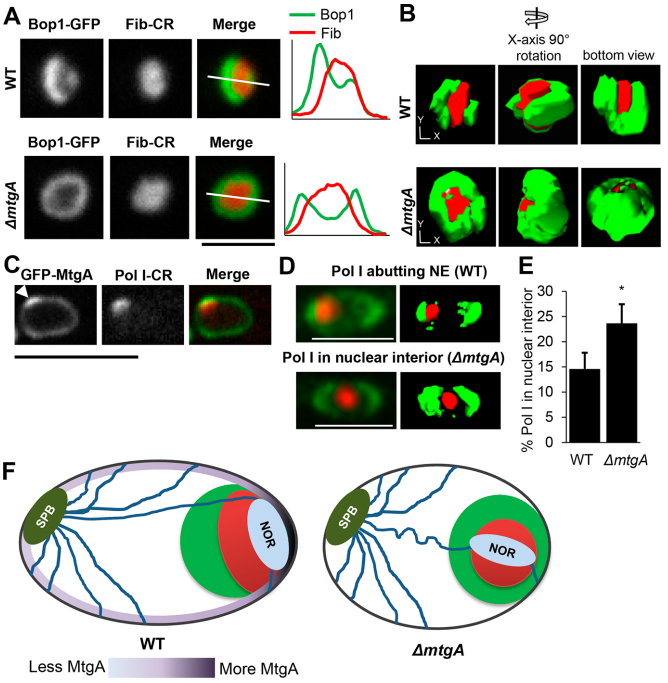

FIGURE 6: MtgA is required to maintain the relative spatial arrangement of nucleolar components. (A) Representative 1 × 1–binning single-confocal-slice images showing the distribution of Bop1-GFP with respect to Fib-CR in WT (CDS777) and Δ*mtgA* cells (MC267). Right, pixel profiles for Bop1 (green) and fibrillarin (red). Scale, 1 μm. (B) Three-dimensional isosurface renderings of Bop1 (green) with respect to fibrillarin (red) in WT and Δ*mtgA* cells from A. (C) GFP-MtgA localization in conjunction with Pol I–CR (strain MC176). Arrowhead indicates the NE region with MtgA concentration, which corresponds to Pol I–CR location at the NE. Imaging collected at 1 × 1 binning. (D) Pol I–CR distribution with respect to Gle1-GFP in WT (strain MC260; top) and Δ*mtgA* (strain MC259; bottom) nuclei, with isosurface rendering for each nucleus to the right. (E) Quantitation of Pol I nuclear interior localization in WT ($n = 233$) and Δ*mtgA* ($n = 317$) nuclei. (F) Model for the nucleolar architecture phenotype in Δ*mtgA* cells. In WT cells, the NOR is at the NE, where there is more MtgA. This spatially positions nucleolar components such that fibrillarin is cradled by Bop1. In Δ*mtgA* cells, the NOR has lost some association with the NE, and fibrillarin now takes up a more central distribution with respect to Bop1, which almost completely surrounds fibrillarin. Scale bar, 5 μm.

slightly, by 18%. To better understand what domains of MtgA might affect nuclear shape, we compared the shape of nuclei during G2 in each of the endogenous CR-MtgA truncation mutant strains (Figure 5B). Although deletion causes rounding of nuclei, several of the strains having truncated versions of MtgA cause the opposite affect, generating more oblong nuclei. Oblong nuclei were seen only in strains having truncated versions that could integrate into the INM. All other truncation mutants of MtgA had rounder G2 nuclei than wild type, including mutants that were targeted to the outer NE/ER (Figure 5B).

MtgA maintains spatial organization of nucleolar proteins

In *A. nidulans*, as in yeast cells, kinetochores cluster at the spindle pole body (SPB) during interphase (Wigge and Kilmartin, 2001; Yang *et al.*, 2004). The SPB is embedded in the NE in a position typically opposite to the nucleolus, which is located adjacent to the NE at the other end of the nucleus. The ribosomal DNA (rDNA) region forming the nucleolar-organizer region (NOR) in *A. nidulans* is located on the long arm of chromosome V (Brody *et al.*, 1991; Clutterbuck and Farman, 2008). The nucleolus is generated around the NOR, with the single NOR generating one nucleolus per nucleus. The nucleolar structure can be divided into three subregions. The fibrillar center (FC) and dense fibrillar (DF) regions are close to the NOR, whereas the granular component (GC) lies more at the nucleolar periphery (Boisvert *et al.*, 2007). We previously reported the spatial arrangement of fibrillarin (a component of the FC/DF region) with respect to Bop1 (a component of the GC; Ukil *et al.*, 2009). In wild-type (WT) cells, fibrillarin (Fib-CR) is cradled by Bop1 (in 61 of 74 nucleoli analyzed; 82.4%), and the Bop1-GFP signal therefore displays an internal "shadow" that is occupied by fibrillarin (Figure 6A, WT). However, in *mtgA*-deleted cells, fibrillarin occupies a more central position and is surrounded evenly by Bop1 (in 65 of 70 nucleoli analyzed; 92.9%; Figure 6A, Δ*mtgA*). Three-dimensional renderings of nucleoli in WT and *mtgA*-deleted cells were completed. In WT nucleoli, fibrillarin is surrounded by Bop1 in a cup-shaped manner, leaving some fibrillarin surfaces less covered

by Bop1 (Figure 6B, WT). In contrast, Bop1 almost entirely surrounds fibrillarin in *mtgA*-deleted strains (Figure 6B, Δ*mtgA*).

Because the nucleolus is built around NORs, we tracked the NOR to investigate its relationship with MtgA. To enable live-cell imaging of the NOR, we imaged endogenously tagged Pol I (Pol I–CR), which associates specifically with the NOR (Boisvert *et al.*, 2007; Ukil *et al.*, 2009). Within WT nuclei, Pol I–CR locates as a focus toward the NE at the nuclear periphery, as does the nucleolus. In 37% of 265 nuclei observed, MtgA was observed to concentrate at distinct regions of the NE, with the majority of these nuclei (79%) having MtgA concentrations at the NE region to which Pol I–CR also associates (Figure 6C, arrowhead). This result suggested that MtgA might be required for the location of Pol I or vice versa. If MtgA is involved in locating Pol I within the nucleus, then deletion of MtgA could influence the location of Pol I. Of interest, Pol I localizes away from the NE at a higher frequency in MtgA-deleted cells than in wild-type cells (Figure 6, D and E). Collectively the data support a model in which wild-type nuclei have their NOR in regions of the NE with higher concentrations of MtgA (Figure 6F). This in turn influences the spatial arrangement of fibrillarin and Bop1. In *mtgA*-deleted cells, the NOR would dissociate from the NE, thereby shifting fibrillarin distribution more to the nuclear interior and become more evenly surrounded by Bop1.

Increased MtgA expression alters nuclear shape and size and modifies compartmentalization of the nucleolus

MtgA deletion results in smaller, rounder nuclei, suggesting that it might play a role in controlling nuclear size. If this were true, excess MtgA would potentially result in larger nuclei. To test this, we expressed extra GFP-MtgA under the transcriptional control of the inducible *alcA* promoter (Waring *et al.*, 1989; Felenbok, 1991). When grown in glycerol (nonrepressive and noninductive for *alcA*), GFP-MtgA levels increase over time, with the induced GFP-MtgA initially distributing quite evenly around the NE (Figure 7A). As cells accumulate higher levels of GFP-MtgA, it starts to localize around the NE unevenly, resulting in a more intense accumulation around a specific nuclear compartment (Figure 7B). When the *alcA*-driven expressed GFP-MtgA displays this localized accumulation, its overall nuclear signal intensity is on average fivefold greater than that of GFP-MtgA expressed from its native locus (Figure 7C). In addition, whereas the null had an 18% reduction in nuclear volume, the overexpression caused a 42% increase in nuclear volume.

Costaining cells with the green fluorescent membrane dye DiOC6(3) (Koning *et al.*, 1993; Saunders *et al.*, 2010) showed that MtgA accumulations correspond to membranous structures (Figure 7D). We found the compartment around which extra MtgA accumulates to be within the nucleus when we observed single confocal *Z*-sections (Figure 7E). Based on its general size and location to one side of the nucleus, the subnuclear region to which excess MtgA accumulates looked like it could be the nucleolus. This was confirmed by monitoring extra MtgA in a strain expressing fibrillarin-CR, showing that the nucleolus was within the nuclear compartment around which MtgA accumulated in 112 of 137 (~82%) nuclei observed (Figure 7F). The remaining 18% of nuclei had a small portion of either the nucleolus or nucleoplasm within the intranuclear compartment (unpublished data). Of note, the intranuclear MtgA-surrounded compartment was largely devoid of Nup49-CR signal (Figure 7G), indicating that NPCs are excluded from the MtgA membrane within nuclei.

To determine how the nucleolus was surrounded by MtgA, we used live-cell imaging during the transition from general NE accumulation of excess MtgA to its preferential accumulation around the nucleolus. A consistent pattern was observed, starting with the NE restricting in around the nucleolus almost to the point of the nucleolus being budded off from the rest of the nucleus (Figure 8A, 12-min arrowheads). In the second phase, additional MtgA accumulated in the NE region at the restriction point between the nucleolus and the rest of the nucleus (Figure 8A, times 16–20 min). In the final stage, extra MtgA was seen to expand from the restriction point and move around to engulf the entire nucleolus, often displaying a cup-like intermediary configuration (Figure 8A, times 20–36 min). The process led to extra MtgA surrounding the nucleolus at a higher level than in the rest of the NE (Figures 7, B, D, and E, 8, A and B, 9A, and 10, A and B). The process of NE expansion upon MtgA overexpression is microtubule independent—nuclei treated with the microtubule poison benomyl were able to form enlarged nuclei and accumulated MtgA in the NE (Supplemental Figure S3).

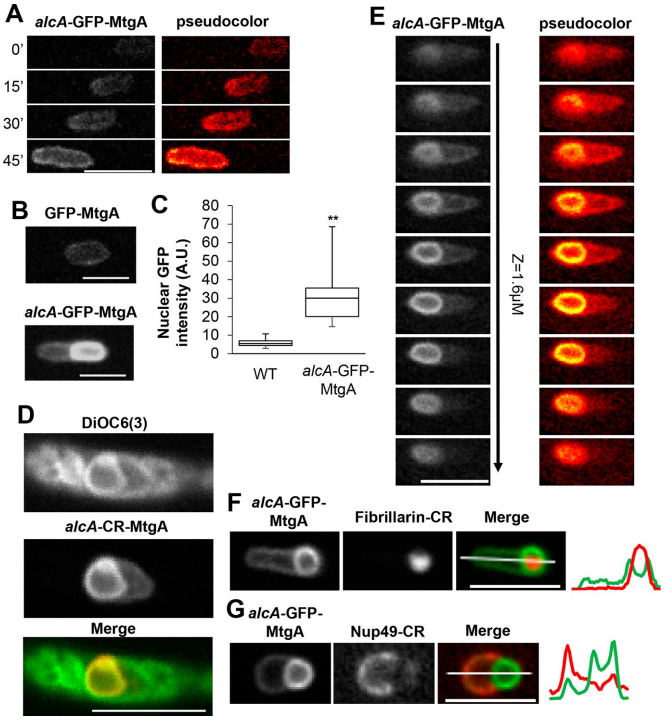

FIGURE 7: MtgA levels affect NE expansion and nuclear compartmentalization. (A) Images of *alcA*-GFP-MtgA levels increasing over time during growth in glycerol (strain MC244). MtgA uniformly localizes around the NE. Pseudocolor image of the same montage shows more clearly increasing MtgA signal specifically at the NE over time. (B) Nuclear shape in WT (GFP-MtgA, strain SO1138) vs. MtgA-overexpressing (*alcA*-GFP-MtgA, strain MC244) cells reveals accumulation of MtgA at a specific NE compartment. Identical exposures were used for GFP-MtgA and *alcA*-GFP-MtgA. (C) GFP-MtgA signal levels in WT vs. MtgA-overexpressing cells ($n > 25$ for each condition, $^{**}p < 0.01$). (D) Single confocal slice of strain MC252 with membranes costained with DiOC6(3) after growth in glycerol to overexpress *alcA*-CR-MtgA. (E) Single confocal slices through *z* in an MtgA-overexpressing nucleus reveals that the NE compartment is intranuclear and in the same plane as the rest of the nucleus. Pseudocolor image of the same montage is shown to better visualize the low-level signals. (F) Single confocal slice depicting *alcA*-GFP-MtgA in conjunction with the nucleolar marker fibrillarin-CR in strain MC232. Right, pixel profile. (G) Single confocal slice depicting *alcA*-GFP-MtgA in conjunction with the NPC marker Nup49-CR (MC213), showing NPCs are excluded from the MtgA membrane within nuclei. Right, pixel profile. Scale bar, 5 μm.

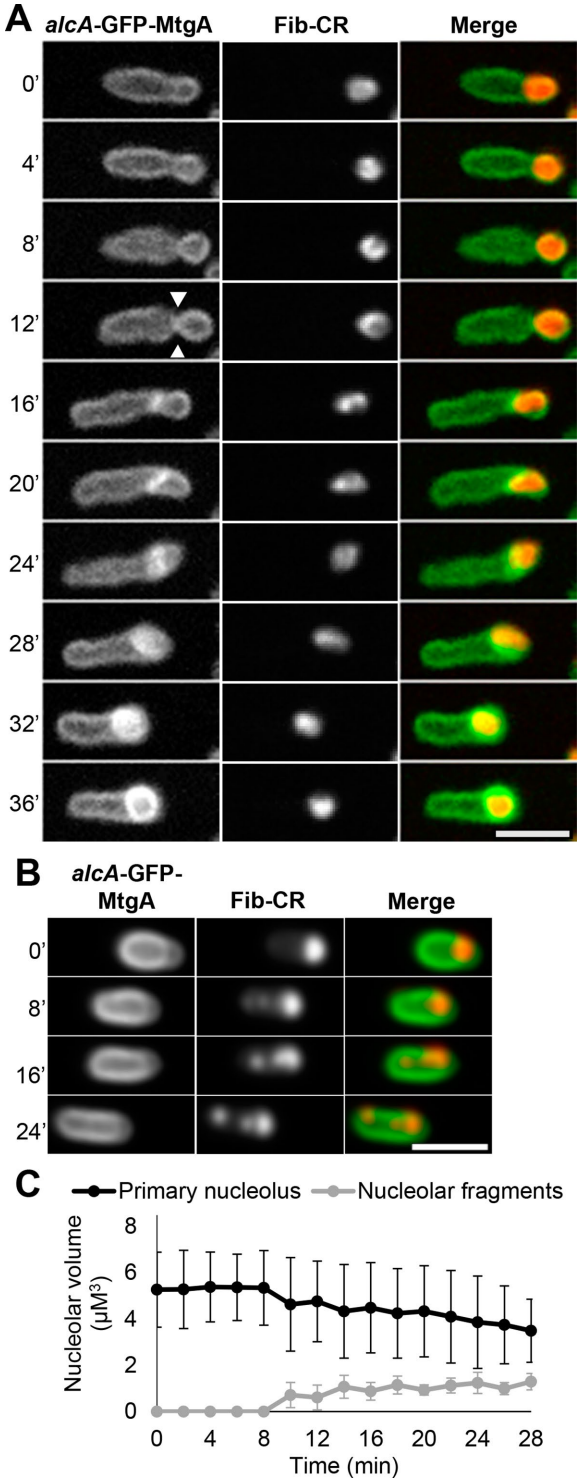

FIGURE 8: Excess MtgA separates the nucleolus into an intranuclear compartment and results in nucleolar fragmentation. Live-cell microscopy of *alcA*-GFP-MtgA in conjunction with fibrillarin-CR, strain MC232. (A) Formation of the intranuclear compartment around the nucleolus. The NE restricts (12 min, arrowheads) around the nucleolus, followed by accumulation of MtgA at the junction between the nucleolus and the rest of the nucleoplasm (16–24 min). MtgA then spreads back around the nucleolus (24–32 min) until it apparently surrounds the nucleolus (36 min). (B) Formation of multiple nucleolar foci upon induction of GFP-MtgA. Initially, there is one fibrillarin signal in the nucleus (time point 0 min), and then fibrillarin foci start to appear (8–24 min). (C) Nucleolar volume vs. time in MtgA-overexpressing cells. The primary nucleolus decreases in volume concomitantly with the appearance and increase in volume of secondary nucleoli, indicating that the parental nucleolus ($n = 9$) likely undergoes fragmentation. Scale bar, 5 μm.

Wild-type interphase nuclei of *A. nidulans* contain a single nucleolus with a single focus of fibrillarin. In contrast, we observed two or more fibrillarin nucleolar signals in 27 of 114 (~24%) nuclei with excess MtgA (Figure 8B). We found no correlation between multiple nucleolar signals and preferential accumulation of MtgA around the nucleolus, as multiple nucleolar signals were also observed in nuclei with an even MtgA distribution around the NE (unpublished data). During this process, the parental nucleolar signal for fibrillarin was reduced (Figure 8C), indicating that fragmentation of the parent nucleolus might generate the additional nucleolar signals.

The observed effects on fibrillarin distribution could be the result of altered distribution of the NOR. As described previously, GFP-MtgA concentrates more at the NE region to which Pol I–CR associates, and lack of MtgA alters Pol I location within the nucleus. Consistent with extra MtgA also being able to influence the location of Pol I, additional MtgA was found to dramatically influence the distribution of Pol I (Figure 9A). Instead of Pol I–CR locating to a distinct perinuclear focus as seen in WT cells, in nucleoli with excess GFP-MtgA enriched around them, Pol I is located in curved structures and often as a ring around the periphery of the nucleolus (Figure 9, A and B, at 6 min). In addition to the more circular configurations, in some nuclei, Pol I–CR appears in a more linear manner (Figure 9A, top). The circular and linear Pol I configurations are unique to nuclei accumulating excess MtgA and are absent from WT nuclei. Abnormal Pol I configurations were observed in 62.5% of 128 MtgA-overexpressing nuclei, compared with 0% of 92 wild-type nuclei. The findings suggest that there is an affinity between MtgA and Pol I or its associated proteins and/or nucleic acids. Live-cell imaging provided further evidence for this, as with time, we observed an association between excess accumulation of MtgA and the locations of Pol I–CR as its location within the nucleolus changed over time (Figure 9B; compare Pol I–CR localization to regions of high MtgA demarcated by arrows in the pseudocolor panel at time points 0, 15, and 21 min).

Collectively our findings from MtgA overexpression and deletion experiments suggest an affinity between MtgA and a component(s) of the nucleolus that can affect nucleolar architecture when levels of MtgA are altered.

Excess MtgA results in redistribution of an integral membrane ER protein into nuclei

Nuclear invaginations of the NE can form from the INM alone or from the entire NE containing both INM and ONM proteins and NPCs. We therefore monitored the effects of excess GFP-MtgA on the levels and location of Erg24, a transmembrane protein of the ER containing eight TMDs. Typically, NE and ER marker proteins colocalize around the NE, as the ER is contiguous with the ONM, as can be seen for MtgA and the ER marker Erg24 (Figure 10A, WT, arrows). Neither locates to the nuclear interior, and only Erg24-CR is present in the cytoplasmic ER (Figure 10A, WT, asterisk). However, when the expression of MtgA is increased, the locations of Erg24-CR are markedly modified such that some of it colocalizes with GFP-MtgA within nuclei around the nucleolus (Figure 10A, *alcA*-MtgA, arrowhead. Note that the exposure for GFP-MtgA was 200 and 80 ms for the *alcA*-GFP-MtgA cell). Live-cell imaging during GFP-MtgA accumulation around the nucleolus revealed that some Erg24-CR located with MtgA as it first locates to the restriction point

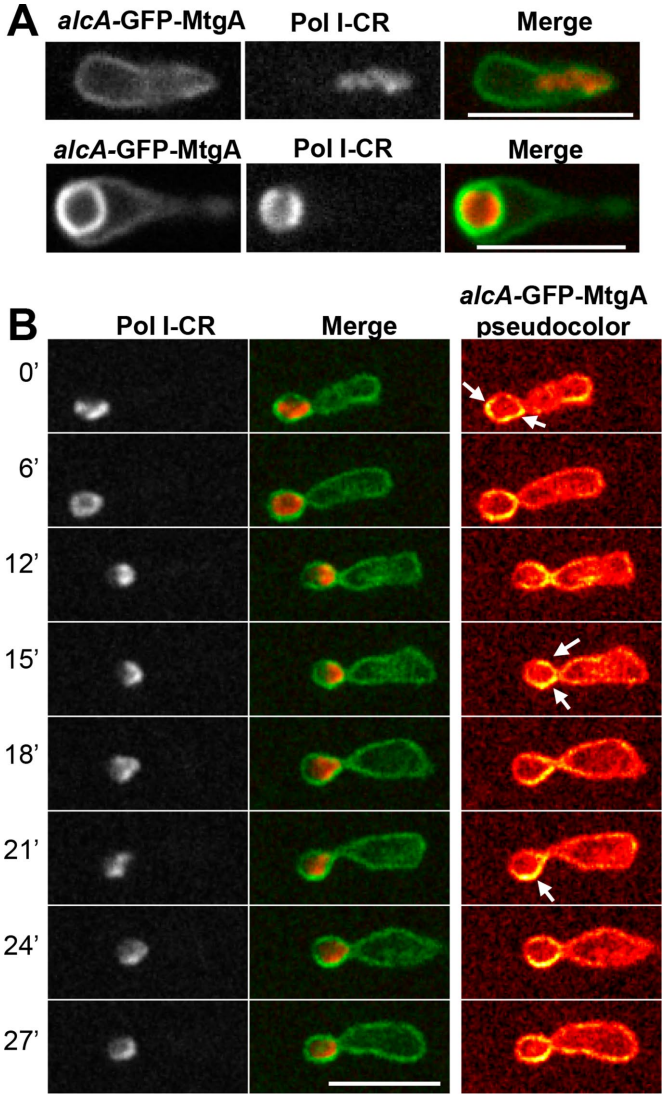

FIGURE 9: Altered Pol I distribution in MtgA-overexpressing cells. (A) Pol I–CR distribution in cells overexpressing extra MtgA (strain MC249). Two examples. Pol I–CR is seen as a linear extension in the top example, where excess MtgA is evenly distributed across the NE. In the bottom nucleus, Pol I–CR is seen in a circular configuration within the nucleolus around which excess MtgA has accumulated. (B) Time-lapse imaging of *alcA*-GFP-MtgA–overexpressing cells in conjunction with Pol I-CR (strain MC249). Pseudocolor of the green channel to the right. Pol I–CR distribution and MtgA concentration at the NE largely coincide as the signals move around the nucleolar region over time (compare Pol I–CR distribution within the nucleolus to MtgA concentrations at the NE, depicted by arrows in pseudocolor). Scale bar, 5 μm.

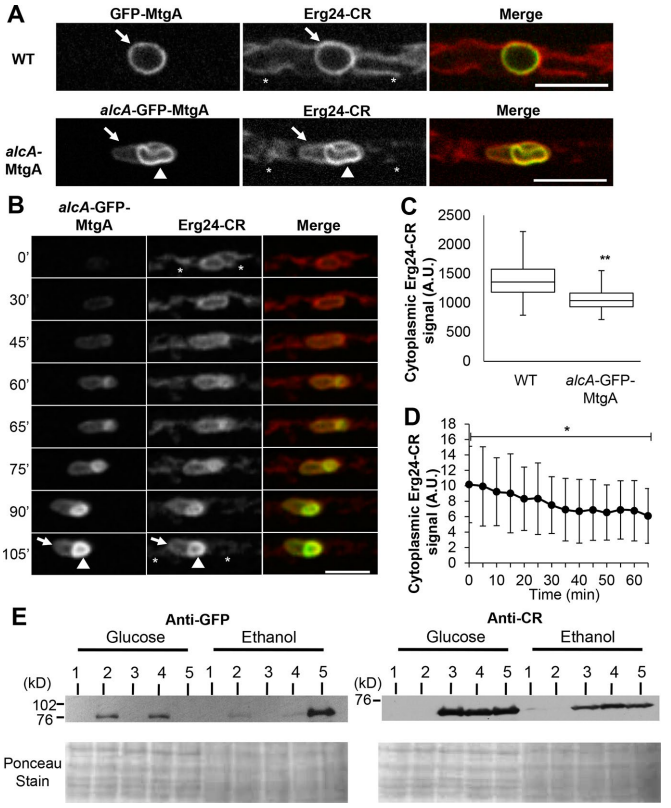

FIGURE 10: Excess MtgA accumulation around the nucleolus also results in the redistribution of an ER membrane marker protein around the nucleolus. (A) Single 1 × 1–binning confocal slice of GFP-MtgA in combination with a marker for the ER membrane (Erg24-CR) in WT (MC263) and *alcA*-GFP-MtgA (MC244) cells. Exposure time is 200 ms for GFP-MtgA and 80 ms for *alcA*-GFP-MtgA. Arrow indicates localization around the nuclear periphery. Arrowhead, localization in the nuclear interior around the nucleolus. Asterisk, Erg24-CR signal in the cytoplasm. (B) Time-lapse imaging of Erg24-CR in *alcA*-GFP-MtgA cells, showing that nuclear Erg24-CR levels increased with MtgA, first to the restriction point and subsequently around the nucleolus. A reduction in cytoplasmic Erg24 signal over time with an increase in GFP-MtgA signal is also seen. Arrow indicates localization around the nuclear periphery; arrowhead, localization in the nuclear interior around the nucleolus; and asterisk, Erg24-CR signal in the cytoplasm. (C) Box-and-whiskers plot of Erg24 cytoplasmic signal intensities in WT ($n = 61$, $^{**}p < 0.01$) and *alcA*-GFP-MtgA ($n = 57$) cells. Line inside boxes denotes median value. (D) Cytoplasmic Erg24-CR signal intensity vs. time ($n = 20$, $^{*}p < 0.05$) in nuclei upon induction of *alcA*-GFP-MtgA. (E) Western blots probing for GFP and CR from cells grown in either *alcA*-repressing glucose or inducing ethanol medium, as indicated. Loading order: 1), negative control (strain SO451); 2), GFP-MtgA only (SO1064); 3), Erg24-mCherry only (HA455); 4), GFP-MtgA and Erg24-mCherry (MC263); and 5), *alcA*-GFP-MtgA and Erg24-mCherry (MC244). Erg24-CR levels remain the same in both GFP-MtgA and *alcA*-GFP-MtgA strains (compare lane 4 to lane 5, anti-CR, ethanol); however, GFP-MtgA levels are noticeably higher in the *alcA*-GFP-MtgA strain (compare lane 4 to lane 5, anti-GFP, ethanol). Scale bar, 5 μm.

and subsequently spreads around the nucleolus (Figure 10B, 105-min arrowheads). During relocation of Erg24 into nuclei, we noticed that its cytoplasmic levels decrease compared with WT cells (Figure 10C). Quantitation of the cytoplasmic Erg24-CR signal intensity over the course of MtgA up-regulation across a population of cells showed a statistically significant decrease in cytoplasmic Erg24 levels (Figure 10D; $n = 20$). Western blot analysis revealed no difference in overall Erg24-CR levels between WT and MtgA-overexpressing cells (Figure 10E). This analysis indicates that nuclear invaginations generated via excess MtgA cause relocation of a transmembrane protein from the ER into the nuclear interior.

Elevated MtgA results in asymmetric two-step mitotic NE division

Considering the dramatic changes in nuclear architecture caused by extra MtgA, we wanted to understand what effects, if any, excess MtgA might have on mitosis. Monitoring DNA segregation using

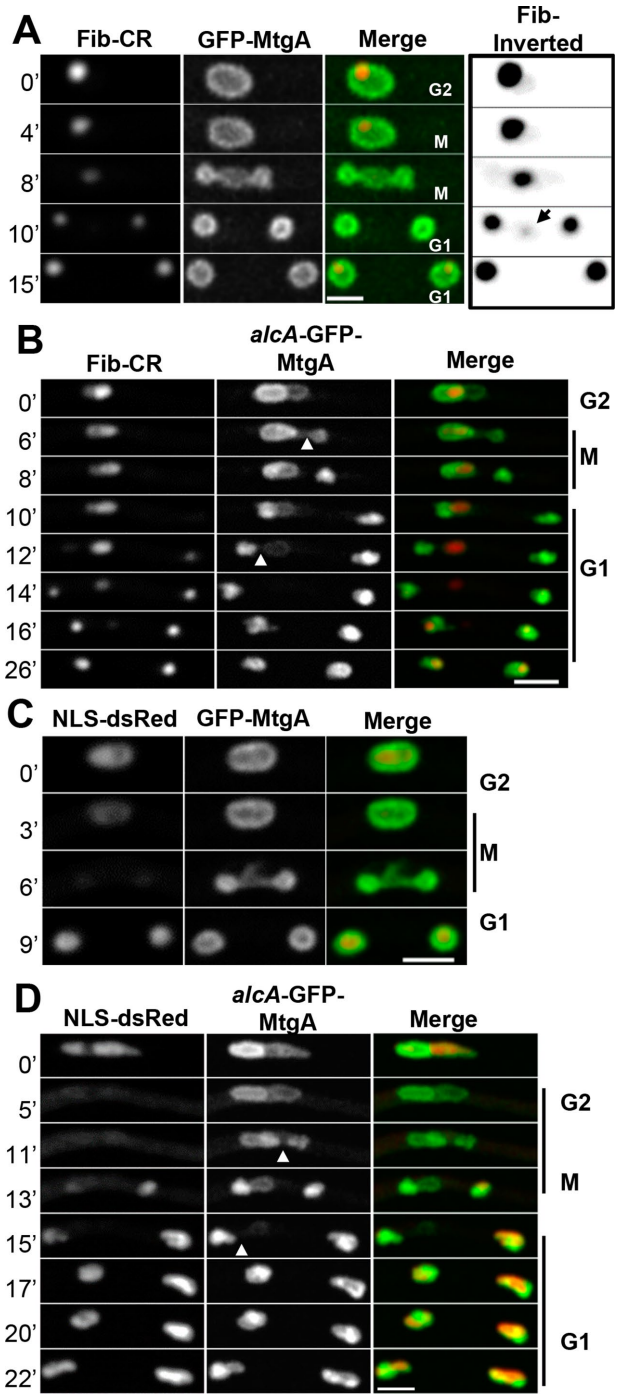

FIGURE 11: Mitotic dynamics in MtgA-overexpressing cells. (A) Time-lapse imaging of GFP-MtgA expressed from its native promoter, showing simultaneous double restriction of the NE on either side of the nucleolus marked by Fib-CR (Strain MC271) during anaphase (time point 8 min). The nucleolus undergoes disassembly in the cytoplasm (10 min; arrow in Fib-inverted points to disassembling nucleolus) and subsequent import into the newly formed nuclei (10, 15 min). (B) Time-lapse imaging of *alcA*-GFP-MtgA in conjunction with Fib-CR (strain MC232), showing that the NE undergoes a two-step restriction of the NE (first at time point 6 min and then at 12 min, indicated by arrowheads) before the nucleolus is released into the cytoplasm for disassembly and subsequent nuclear import (14–26 min). (C) GFP-MtgA followed over time in conjunction with NLS-dsRed (strain MC313). Mitotic entry is marked by dispersal of NLS-dsRed. At the point of double restriction of the NE, NLS-dsRed is absent from the nucleus (time point 6 min) and is subsequently imported equally into the new G1 nuclei (9 min). (D) In strain MC248 expressing *alcA*-GFP-MtgA, NLS-dsRed is dispersed upon entry into mitosis as normal. Two daughter nuclei are then generated sequentially, as indicated by the arrowheads (11 and then 13 min). Because the daughter nucleus to the right is generated first, it accumulates more NLS-dsRed. Scale bar, 5 μM.

histone H1 revealed no major defects (Supplemental Figure S4), consistent with the lack of obvious growth defects associated with excess MtgA (unpublished data). We did, however, observe defects in the behavior of the NE during mitosis. As described earlier (Figure 3A), after anaphase, the NE restricts simultaneously on either side of the nucleolus, transiently forming three structures—the centrally located nucleolus and two daughter nuclei (Figure 11A, 8 min). However, in nuclei with extra GFP-MtgA accumulated around their nucleolus, the NE first restricts only around one of the daughter nuclei (Figure 11B, arrowhead) during mitosis. This daughter nucleus was the one located within the NE region having lower levels of GFP-MtgA (Figure 11B). The other daughter nucleus was generated several minutes after the first by a second NE restriction that occurred between itself and the nucleolus (Figure 11B, 12-min arrowhead; see also Figure 11D, 15-min arrowhead). The two sequential NE restrictions seen in nuclei with excess GFP-MtgA suggest that the first generated nucleus might enter G1 before the second. By monitoring the nuclear reimport of NLS-DsRed, a hallmark of entry into G1 (Suelmann *et al.*, 1997; De Souza *et al.*, 2004), we observe similar levels of NLS-DsRed imported into newly formed daughter nuclei in wild-type cells (Figure 11C). In contrast, in MtgA-overexpressing cells, earlier and higher levels of NLS-DsRed import are observed in the first generated daughter nucleus (Figure 11D). Of interest, this discrepancy in nuclear levels of G1 NLS-DsRed was not seen for nucleolar proteins (Figure 11B). This is most likely because an additional limiting factor in G1 nuclear import of nucleolar proteins occurs when they get released into the cytoplasm. Because this occurs after the second NE restriction, both daughter nuclei have similar potential for reimporting the released cytoplasmic nucleolar proteins. Therefore, although the sequence and timing of some mitotic events are different in nuclei in which MtgA has accumulated, mitosis is successfully completed.

DISCUSSION

MtgA is the *A. nidulans* orthologue of Bqt4 and facilitates meiosis independently of mitotic telomere NE tethering

We identified the *A. nidulans* orthologue of fission yeast Bqt4, an INM protein that in fission yeast is involved in tethering telomeres to the NE during vegetative growth and also meiotic recombination (Chikashige *et al.*, 2009). The *Aspergillus* Bqt4 orthologue was identified via affinity purification of the RNA export NPC protein Gle1 and found to play an essential role in tethering Gle1 to the mitotic NE, as discussed later. We named this previously unstudied protein in *A. nidulans* MtgA for "mitotic tether for Gle1 A." Like Bqt4, MtgA contains an APSES-type DNA-binding domain and a C-terminal TM domain. Both Bqt4 and MtgA require an NLS upstream of the TM domain for exclusive targeting to the NE. We therefore suggest that MtgA is inserted into the INM like Bqt4 (Chikashige *et al.*, 2009; Chikashige *et al.*, 2010). Bqt4/MtgA proteins are conserved among both the Ascomycota and Basidiomycota, although *S. cerevisiae* appears not to have an orthologue.

MtgA, like Bqt4, is required for normal levels of meiotic recombination, but it is not required for mitotic telomere tethering to the

NE. Mitotic telomere tethering to the NE in fission yeast is required for subsequent telomere clustering to form the bouquet arrangement of chromosomes during meiotic prophase. Our data suggest, however, that the role of MtgA in meiotic recombination does not involve telomere NE tethering before meiosis. Instead, the observed meiotic defects in MtgA-deleted cells might involve the new functions we defined for this class of protein, including mitotic-specific NE tethering of Gle1 and modulation of nuclear and nucleolar architecture.

MtgA is required for mitotic-specific tethering of Gle1 to the NE

Gle1 is an mRNA export factor expected to disperse from NPCs during the partially open mitosis of *A. nidulans*; however, it remains at the NE during mitosis (Osmani *et al.*, 2006a; Ukil *et al.*, 2009). This paradox has been solved: we demonstrate that Gle1 associates with NPCs during interphase but during mitosis, transitions to locate at the INM via MtgA. During mitosis, Gle1 remains tethered to the NE via MtgA and returns to NPCs after mitosis in G1. Thus, although Gle1 remains at the NE throughout the cell cycle, it does so at two distinct locations. To our knowledge, this is the first reported instance of a protein being tethered at two different regions of the NE in a mitotically regulated manner.

The dispersal of Gle1 from the mitotic NE caused by *mtgA* deletion does not result in obvious mitotic phenotypes, although we have not tested the fidelity of mitotic events in the absence of *mtgA*. This suggests that Gle1 at the mitotic NE has nonessential functions that are perhaps also not readily visualized. As an example, it could be required to help remove RNA molecules remaining in the nucleus and/or nucleolus during mitosis. However, this work does provide novel insights into the mitotic NE tethering of Gle1, and it will be interesting if similar mitotic-specific locations occur in other species and if this might play roles in the disease states associated with Gle1 mutations (Nousiainen *et al.*, 2008; Glass *et al.*, 2016).

MtgA levels dramatically modify nuclear architecture

In addition to its roles in meiosis and mitotic tethering of Gle1 to the NE, MtgA was also found to affect dramatically nuclear architecture when either deleted or in excess. The most obvious defect caused by lack of *mtgA* was the formation of slightly smaller, rounder nuclei. Truncation gene replacement experiments indicate that integration of MtgA into the INM is involved in its ability to maintain the size and shape of nuclei.

In addition to causing rounder and smaller nuclei, deletion of MtgA also alters the internal organization of the nucleolus. The nucleolus is assembled around NORs and contains a distinctive internal architecture to which specific proteins locate. For example, fibrillarin occupies a centrally located position within the nucleolus and is surrounded unevenly by Bop1. However, in the absence of MtgA, the spatial relationship between fibrillarin and Bop1 is changed such that fibrillarin is more evenly surrounded by Bop1 (Figure 6A). This shows that MtgA is required to maintain the distinctive distribution of proteins within the nucleolus. One potential mechanism is modification of the location of the NOR, an idea further supported by the effects caused by excess MtgA.

Because lack of MtgA generates smaller nuclei and modifies the architecture of the nucleolus, we anticipated that extra MtgA might enlarge nuclei and perhaps change the structure of the nucleolus. These expectations were fulfilled. Nuclei became enlarged as excess MtgA initially accumulated evenly in their NE. However, these nuclei apparently have a limit on the size to which they can enlarge. This is suggested by the fact that, as nuclei accumulated further MtgA, they stopped enlarging and started to accumulate the extra MtgA specifically around their nucleoli. During this process, the nucleolus became largely surrounded by MtgA and its associated membrane (Figure 7). Although several studies showed that induced expression of proteins (Wright *et al.*, 1988; Ralle *et al.*, 2004; Malhas *et al.*, 2011; Masuda *et al.*, 2016), including those of the INM (Ma *et al.*, 2007; Friederichs *et al.*, 2011; Goto *et al.*, 2014), can cause elaboration of intranuclear membranes, none that we know of revealed a specific expansion of intranuclear membrane around the nucleolus.

Several questions arise from the finding that excess MtgA accumulates specifically around the nucleolus. For example, what is the nature of the intranuclear membrane associated with extra MtgA, and how might it form? The intranuclear MtgA membrane is costained by the lipophilic membrane dye DiOC6(3) and contains a transmembrane ER marker, suggesting that it represents mislocalized NE. This membrane could be generated, at least in part, through redistribution of membrane from the ER, as the cytoplasmic levels of an ER membrane marker decrease during the process. However, the intranuclear MtgA membrane does not represent a complete NE because it lacks NPCs.

There are two possibilities for how the excess MtgA-induced intranuclear membrane might be formed. It could represent an expansion of just the INM to which ONM proteins are now able to locate. Alternatively, the MtgA-promoted intranuclear membrane could represent both the INM and ONMs from which NPCs are excluded. Of further interest, and most notably, accumulation of MtgA induces the NE to invaginate into the nucleoplasm specifically at the interface between the nucleoplasm and nucleolus. This novel yet specific accumulation suggests that MtgA might have a weak affinity for a nucleolar component. Then, as MtgA levels increase within the NE, the net weak nucleolar affinity might accumulate to a level that promotes the NE being pulled in and expanding around the nucleolar surface but not around the bulk DNA. The contact between the INM and nucleolus mediated by excess MtgA potentially could also generate a mechanical barrier to both the movement of NPCs into this NE and the de novo generation of nuclear pores at this NE. This would explain how MtgA accumulation promotes NE invagination around the nucleolus containing ONM and INM proteins but not NPCs.

Further experimentation will be needed to test these working hypotheses, but some findings lend support to the idea that MtgA has weak affinity for the nucleolus. For example, in wild-type cells, MtgA partially concentrates to the NE directly adjacent to the nucleolus, where Pol I also locates (Figure 6C). In addition, without MtgA, the architecture of the nucleolus is modified. Finally, the normal location of Pol I is compromised in both MtgA-lacking and MtgA-overexpressing cells. Our findings therefore collectively indicate that MtgA is required to maintain the normal position of the NOR and nucleolar architecture.

Although we are unaware of other instances of induced intranuclear membranes locating specifically around the nucleolus, studies using *S. cerevisiae* identified the NE adjacent to the nucleolus as a site for induced NE membrane accumulation. In these studies, under conditions that promote extra NE formation (including mitotic delay and induced imbalance in lipid synthesis), the NE expands out from the nucleolus, forming "flares" that extend into the cytoplasm. The expandable NE adjacent to the nucleolus is believed to act as a "membrane sink" allowing the nucleus to accommodate increased NE levels without dramatically increasing nuclear volume (Campbell *et al.*, 2006; Witkin *et al.*, 2012; Meseroll and Cohen-Fix, 2016). We propose that *A. nidulans* deals with the excess NE problem caused

by extra MtgA by incorporating it within nuclei around the nucleolus rather than out into the cytoplasm, such that the extra NE does not uncontrollably affect overall nuclear size, and so it helps to maintain an acceptable nuclear/cell volume ratio (Huber and Gerace, 2007; Meseroll and Cohen-Fix, 2016). By exclusion of NPCs from this extra membrane, normal levels and direction of nuclear transport presumably can also be maintained.

It is surprising that turning the nucleolus into a largely membrane-bound organelle, as occurs upon MtgA accumulation, does not cause clear growth defects. In part, this is probably because the excess MtgA nuclear membrane does not prevent completion of successful mitosis. In spite of this, the mitotic process itself is modified, as daughter nuclei are generated sequentially rather than in unison. This is accompanied by a delay in the normal process of mitotic nucleolar disassembly into the cytoplasm. Because nucleolar disassembly still occurs after daughter nuclei have formed in G1 and reestablished nuclear transport, both subsequently get a relatively equal portion of nucleolar proteins, ensuring faithful nucleolar protein segregation. If indeed the nucleolus is surrounded by membrane, it would be expected that transport of nucleolar products out into the cytoplasm would be hindered. However, because the nucleolus is disassembled and its contents released into the cytoplasm during mitosis, this gives the nucleolus the opportunity to release its products, even if it is membrane bound, once per cell cycle.

The large diversity of nuclear morphologies exhibited across both healthy and diseased cells demonstrates that there are important regulated mechanisms used by organisms to maintain nuclear size and architecture (Zink *et al.*, 2004; Webster *et al.*, 2009; Malhas *et al.*, 2011; Edens *et al.*, 2013; Vukovic *et al.*, 2016). Collectively our work furthers our understanding of how organisms can maintain nuclear architecture and cope with excess nuclear membrane. This study uncovered a novel INM protein–dependent mechanism that expands the NE specifically around the nucleolus, and it will be of interest to know whether a similar mechanism is used in other organisms as a means of maintaining the size of nuclei experiencing NE expansion.

MATERIALS AND METHODS

General techniques

The genotypes of *A. nidulans* strains used in this work are listed in Supplemental Table S1 and were generated using standard techniques (Pontecorvo *et al.*, 1953; Yang *et al.*, 2004; Nayak *et al.*, 2006). *mtgA* was deleted using the *pyrG*^{Af} marker. The deletion construct was generated using fusion PCR followed by transformation of a Δ*nkuA*^{ku70} strain as described previously (Yang *et al.*, 2004; Nayak *et al.*, 2006; Szewczyk *et al.*, 2006) using primers listed in Supplemental Table S2. Deletion of *nup42* and *nup133* was described previously (Osmani *et al.*, 2006a). To generate Rap1-GFP-S-tag, three-way fusion PCR was performed. The GFP–S-tag::*pyrG*^{Af} cassette was first amplified from plasmid pCDS65 (De Souza *et al.*, 2014) using C-terminal tagging primers HP116 and FN01-pyrG (Yang *et al.*, 2004; Liu *et al.*, 2010). The upstream Rap1 targeting sequence was amplified from wild-type DNA using MaC59 and MaC38, whereas the downstream Rap1 sequence, including the stop codon and 3′ untranslated region, was amplified using primers MaC36 and MaC39. MaC38 has an overhang that complements the sequence to primer HP116, whereas MaC39 has an overhang complementing primer FN01-pyrG to enable PCR-directed fusion of the three products. The fusion construct was obtained by amplifying the three PCR products with primers MaC59 and MaC36. The fusion construct was used for strain SO451 transformation. Site-specific integration was confirmed via diagnostic PCR with primers MC34 and MC37. Because MtgA has a transmembrane domain at its C-terminus, fluorescent protein tagging of MtgA was done at the N-terminus to avoid possible disruption of localization and folding of MtgA and/or the fluorescent protein arising from the membrane topology of MtgA. The exception to this is MtgAΔTMD-GFP-S-tag (see later discussion), which lacked its transmembrane domain and was tagged C-terminally. N-terminal fluorescent protein fusion constructs lacked selection markers and were used for transforming Δ*mtgA* strains marked by the wild-type *pyrG* allele from *Aspergillus fumigatus* (*pyrG*^{Af}), which complements the mutant *pyrG89* allele in the genetic background. After transformation of Δ*mtgA* strains, counterselection was done using 1 mg/ml 5-fluoroorotic acid (5-FOA; toxic to *pyrG*$^{+}$ strains; US Biological, Salem, MA) added to yeast extract/glucose agar medium containing uridine and uracil to select for transformants that incorporated the N-terminal fusion constructs and evicted *pyrG*^{Af}. Primers AO359 and AO390 were used to check for site-specific integration. For generation of protoplasts from *pyrG*$^{+}$ strains to enable transformation, cells were grown initially in yeast extract/glucose medium at 32°C with shaking until emergence of germ tubes was observed (shmoo cells) and their cell wall digested as follows. The cells were centrifuged and washed with 0.55 M KCl and 50 mM citric acid, pH 6.5, and transferred to a solution consisting of 10 mg/ml VinoFlow FCE (Novozymes, Bagsværd, Denmark) or 15 mg/ml Vinotaste (Novozymes) in 0.55 M KCl and 50 mM citric acid. Cells were protoplasted under conditions that impeded further growth (unpublished data), and protoplasts were collected as per standard techniques (Osmani *et al.*, 2006b). Alternatively, *pyrG*$^{+}$ strains were protoplasted from mycelia as described previously (Szewczyk *et al.*, 2006) with minor modifications. The GFP-MtgA tagged strain was generated as described using three-way fusion PCR (Szewczyk *et al.*, 2006) and primers listed in Supplemental Table S2. Upstream and downstream *mtgA* sequences were generated using primers AO390/AO388 and AO391/AO359, respectively. The *gfp* sequence was amplified from plasmid pFN03 (Yang *et al.*, 2004) using primers HP108 and KF043. The construct derived from fusion of *gfp* and upstream and downstream *mtgA* sequences was generated with primers AO358/AO389, transformed into SO451, and PCR confirmed using primers AO359/AO390. To generate *alcA*-GFP-MtgA strains, we used the pAL5 plasmid vector system (Doonan *et al.*, 1991), which allows for in-frame insertion of the gene of interest under the control of the inducible *alcA* promoter (Waring *et al.*, 1989; Felenbok, 1991). pAL5 was modified by cloning the fragment *Kpn*I-*Nsi*I-*gfp*-*Bgl*II-*Nhe*I into the *Kpn*I and *Nhe*I sites of the pAL5 backbone that are situated downstream of the *alcA* promoter such that GFP is under the control of the *alcA* promoter. This new plasmid, pAL5-5′GFP, was generated by Colin De Souza and kindly gifted for use in this study. The gene of interest can be inserted in-frame into a unique polylinker after the GFP sequence that contains *Nhe*I-*Sma*I-*Bam*HI such that it is N-terminally GFP tagged under the *alcA* promoter. The *mtgA* sequence was PCR amplified from a wild-type strain using primers MaC31 (containing an *Nhe*I site) and MaC32 (containing a *Bam*HI site), digested with *Nhe*I and *Bam*HI, and then cloned into the *Nhe*I and *Bam*HI sites on plasmid pAL5-5′GFP to obtain plasmid pMC1. *mtgA* insertion into pMC1 was confirmed by sequencing using primers MaC44, MaC45, MaC46, and MaC47. To generate *alcA*-CR-MtgA, the *gfp* sequence was replaced with an *mCherry* sequence. For this, *mCherry* was amplified using primers MaC87 (having an *Nhe*I site) and MaC88 (having a *Kpn*I site) from pHL85 (Liu *et al.*, 2009) and cloned into the *Kpn*I (upstream of *gfp*) and *Nhe*I (downstream of *gfp*) sites on pMC1 by digesting pMC1 with *Nhe*I and *Kpn*I, checking the size to confirm loss of the *gfp* fragment, and then ligating

with the *Nhe*I plus *Kpn*I–digested *mCherry* sequence to obtain pMC2. Plasmids pMC1 and pMC2 were then used for transformation of SO451 and selection for complementation of *pyrG89*.

Affinity purification and liquid chromatography–tandem mass spectrometry

Gle1–S-tag (strain SO901) and MtgAΔTMD-GFP–S-tag (strain MC107) affinity purifications followed by mass spectrometry were done as previously described (Liu *et al.*, 2010). Full-length MtgA affinity purifications were unsuccessful (unpublished data), and hence a strain expressing a version of MtgA lacking its TMD and C-terminally fused to GFP–S-tag was used for affinity purifications. The MtgAΔTMD-GFP–S-tag construct was generated as described earlier for Rap1-GFP–S-tag. The upstream MtgA sequence was PCR amplified using primers MaC01/MaC24, and the downstream MtgA sequence was amplified using MaC23/MaC04. Primers MaC23 and MaC24 have overhangs priming FN01-pyrG and HP116, respectively. The fusion construct was obtained by amplifying the three PCR products with primers MaC1 and MaC4. The fusion construct was used for SO451 transformation. Site-specific integration was confirmed with primers AO359 and AO390. Expression of S-tag was confirmed by Western blotting using anti–S-tag antibody (Immunology Consultants Laboratory, Portland, OR).

Live-cell imaging

Live-cell imaging and induction of genes regulated by the *alcA* promoter was done as described previously (Govindaraghavan *et al.*, 2014) and additionally using a 100×/1.4 numerical aperture total internal reflection fluorescence objective lens on an Eclipse TE 2000-U (Nikon, Tokyo, Japan) microscope equipped with an UltraView ERS spinning-disk confocal system. Benomyl at 2.4 μg/ml was used to depolymerize microtubules. Cell membranes were visualized by adding 1 μl of 10 mM DiOC6(3) (Sigma-Aldrich, St. Louis, MO) to hyphae grown overnight in 3 ml of medium containing glycerol as a carbon source immediately followed by microscopy.

Bioinformatics

Orthologues of *A. nidulans* KilA-N proteins present in other fungi were identified by BLAST search (blast.ncbi.nlm.nih.gov/Blast.cgi) against species in different fungal families in either the Ascomycota or Basidiomycota. The phylogenetic tree was constructed using MEGA version 7 (Kumar *et al.*, 2016) by aligning sequences using ClustalW with a BLOSUM62 matrix and then generating a maximum-likelihood tree of the alignment.

MtgA domain analysis

mCherry-MtgA and mCherry-MtgA truncations were generated by N-terminal tagging as described. mCherry-MtgA was generated by amplifying mCherry from plasmid pHL85 (Liu *et al.*, 2009) using primers MaC07 and MaC08. This product was fused to flanking products amplified from a wild-type strain using primers MaC01/MaC09 and MaC10/MaC04. The fusion PCR product was subsequently transformed into strain SO1062, and transformants were counterselected by 5-FOA eviction of $pyrG^{Af}$ to obtain strain MC039 (*pyrG89 fwA1; wA3; argB2; pyroA4 ΔnkuA::argB; CR-mtgA chaA1 sE15 nirA14*). DNA from strain MC039 was then used to amplify PCR products for domain analysis. Primers used were $MtgA^{162\text{-}424}$, Mac01/MaC08 and MaC15/MaC04; $MtgA^{217\text{-}424}$, Mac01/MaC08 and MaC20/MaC04; $MtgA^{291\text{-}424}$, Mac01/MaC08 and MaC16/MaC04; $MtgA^{373\text{-}424}$, Mac01/MaC08 and MaC17/MaC04; $MtgA^{1\text{-}404}$, MaC01/MaC18 and MaC03/MaC04; $MtgA^{1\text{-}372}$, MaC01/MaC33 and MaC03/MaC04; $MtgA^{1\text{-}290}$, MaC01/MaC30 and MaC03/MaC04; $MtgA^{1\text{-}216}$, MaC01/MaC02 and MaC03/MaC04; $MtgA\Delta^{291\text{-}372}$, MaC01/MaC50 and MaC51/MaC04; $MtgA^{291\text{-}372}$, MaC01/MaC08, MaC16/MaC33, and MaC03/MaC04. All constructs were transformed into MC090, and counterselected by 5-FOA eviction of $pyrG^{Af}$.

Western blotting

Western analysis was performed as described previously (Osmani *et al.*, 2006a) with the modification that strains were grown in minimal medium using either 55 mM glucose or 1% (vol/vol) ethanol as a carbon source.

Data analyses

Image analyses were carried out using ImageJ software (National Institutes of Health, Bethesda, MD) or Volocity Image Analysis Software (PerkinElmer, Waltham, MA). For Figure 2B, Rap1-GFP nuclear localization was determined for the central focal plane of each nucleus as determined by Nup49-CR distribution. For Figure 5B, nuclear circularity values were calculated during G2 (defined as 6–10 min before onset of nuclear division) for all mutants tested. Three-dimensional renderings in Figure 6B were generated using isosurface renderings with identical settings for each condition using Volocity Image Analysis Software. For Figure 7C, nuclear GFP intensities were calculated after background subtractions for each condition. Erg24-CR cytoplasmic signal intensities in Figure 10 were calculated after background subtraction. Fluorescence intensities and volumes were calculated by identifying objects for desired channels using Volocity Image Analysis Software. Pixel intensity profiles were obtained by drawing indicated regions of interest in ImageJ. Plotting of graphs and statistics was done using Microsoft Excel. Unpaired, two-tailed *t* tests were performed to calculate statistical significance.

ACKNOWLEDGMENTS

We are grateful to all members of the Osmani lab, especially Subbulakshmi Suresh, for assistance with designing and standardizing the $pyrG^{+}$ strain protoplasting technique and Colin De Souza for strains and vectors. We are also grateful to Matthew Johns for assistance with experiments. Jennifer Larson critically read the manuscript, for which we extend our gratitude. We thank Miguel Penalva for sharing his thoughts on this work and kindly gifting strain MAD1543. This work was supported by Grant GM042564 from the National Institutes of Health to S.A.O.

REFERENCES

Boisvert FM, van Koningsbruggen S, Navascues J, Lamond AI (2007). The multifunctional nucleolus. Nat Rev Mol Cell Biol 8, 574–585.

Bolger TA, Folkmann AW, Tran EJ, Wente SR (2008). The mRNA export factor Gle1 and inositol hexakisphosphate regulate distinct stages of translation. Cell 134, 624–633.

Brody H, Griffith J, Cuticchia AJ, Arnold J, Timberlake WE (1991). Chromosome-specific recombinant DNA libraries from the fungus Aspergillus nidulans. Nucleic Acids Res 19, 3105–3109.

Campbell JL, Lorenz A, Witkin KL, Hays T, Loidl J, Cohen-Fix O (2006). Yeast nuclear envelope subdomains with distinct abilities to resist membrane expansion. Mol Biol Cell 17, 1768–1778.

Chikashige Y, Haraguchi T, Hiraoka Y (2010). Nuclear envelope attachment is not necessary for telomere function in fission yeast. Nucleus 1, 481–486.

Chikashige Y, Tsutsumi C, Yamane M, Okamasa K, Haraguchi T, Hiraoka Y (2006). Meiotic proteins bqt1 and bqt2 tether telomeres to form the bouquet arrangement of chromosomes. Cell 125, 59–69.

Chikashige Y, Yamane M, Okamasa K, Tsutsumi C, Kojidani T, Sato M, Haraguchi T, Hiraoka Y (2009). Membrane proteins Bqt3 and -4 anchor telomeres to the nuclear envelope to ensure chromosomal bouquet formation. J Cell Biol 187, 413–427.
Chow KH, Factor RE, Ullman KS (2012). The nuclear envelope environment and its cancer connections. Nat Rev Cancer 12, 196–209.
Clutterbuck AJ, Farman ML (2008). Aspergillus nidulans linkage map and genome sequence: closing gaps and adding telomeres. In: The Aspergilli: Genomics, Medical Aspects, Biotechnology, and Research Methods, ed. GH Goldman and SA Osmani, Boca Raton, FL: CRC/Taylor and Francis, 57–65.
D'Angelo MA, Hetzer MW (2008). Structure, dynamics and function of nuclear pore complexes. Trends Cell Biol 18, 456–466.
De Souza CP, Hashmi SB, Osmani AH, Osmani SA (2014). Application of a new dual localization-affinity purification tag reveals novel aspects of protein kinase biology in Aspergillus nidulans. PLoS One 9, e90911.
De Souza CP, Osmani AH, Hashmi SB, Osmani SA (2004). Partial nuclear pore complex disassembly during closed mitosis in Aspergillus nidulans. Curr Biol 14, 1973–1984.
Doonan JH, MacKintosh C, Osmani S, Cohen P, Bai G, Lee EY, Morris NR (1991). A cDNA encoding rabbit muscle protein phosphatase 1 alpha complements the Aspergillus cell cycle mutation, bimG11. J Biol Chem 266, 18889–18894.
Doucet CM, Talamas JA, Hetzer MW (2010). Cell cycle-dependent differences in nuclear pore complex assembly in metazoa. Cell 141, 1030–1041.
Doye V, Wepf R, Hurt EC (1994). A novel nuclear pore protein Nup133p with distinct roles in poly(A)+ RNA transport and nuclear pore distribution. EMBO J 13, 6062–6075.
Edens LJ, White KH, Jevtic P, Li X, Levy DL (2013). Nuclear size regulation: from single cells to development and disease. Trends Cell Biol 23, 151–159.
Felenbok B (1991). The ethanol utilization regulon of Aspergillus nidulans: the alcA-alcR system as a tool for the expression of recombinant proteins. J Biotechnol 17, 11–17.
Fichtman B, Ramos C, Rasala B, Harel A, Forbes DJ (2010). Inner/outer nuclear membrane fusion in nuclear pore assembly: biochemical demonstration and molecular analysis. Mol Biol Cell 21, 4197–4211.
Folkmann AW, Noble KN, Cole CN, Wente SR (2011). Dbp5, Gle1-IP6 and Nup159: a working model for mRNP export. Nucleus 2, 540–548.
Friederichs JM, Ghosh S, Smoyer CJ, McCroskey S, Miller BD, Weaver KJ, Delventhal KM, Unruh J, Slaughter BD, Jaspersen SL (2011). The SUN protein Mps3 is required for spindle pole body insertion into the nuclear membrane and nuclear envelope homeostasis. PLoS Genet 7, e1002365.
Glass AL, Dawson TR, Wente SR (2016). An amyotrophic lateral sclerosis-linked mutation in *GLE1* alters the cellular pool of human Gle1 functional isoforms. Adv Biol Regul 62, 25–36.
Goto C, Tamura K, Fukao Y, Shimada T, Hara-Nishimura I (2014). The novel nuclear envelope protein KAKU4 modulates nuclear morphology in Arabidopsis. Plant Cell 26, 2143–2155.
Govindaraghavan M, McGuire Anglin SL, Shen KF, Shukla N, De Souza CP, Osmani SA (2014). Identification of interphase functions for the NIMA kinase involving microtubules and the ESCRT pathway. PLoS Genet 10, e1004248.
Guttinger S, Laurell E, Kutay U (2009). Orchestrating nuclear envelope disassembly and reassembly during mitosis. Nat Rev Mol Cell Biol 10, 178–191.
Hatch E, Hetzer M (2014). Breaching the nuclear envelope in development and disease. J Cell Biol 205, 133–141.
Hetzer MW (2010). The nuclear envelope. Cold Spring Harb Perspect Biol 2, a000539.
Huber MD, Gerace L (2007). The size-wise nucleus: nuclear volume control in eukaryotes. J Cell Biol 179, 583–584.
Iyer LM, Koonin EV, Aravind L (2002). Extensive domain shuffling in transcription regulators of DNA viruses and implications for the origin of fungal APSES transcription factors. Genome Biol 3, RESEARCH0012.
Kendirgi F, Barry DM, Griffis ER, Powers MA, Wente SR (2003). An essential role for hGle1 nucleocytoplasmic shuttling in mRNA export. J Cell Biol 160, 1029–1040.
Kendirgi F, Rexer DJ, Alcazar-Roman AR, Onishko HM, Wente SR (2005). Interaction between the shuttling mRNA export factor Gle1 and the nucleoporin hCG1: a conserved mechanism in the export of Hsp70 mRNA. Mol Biol Cell 16, 4304–4315.
King MC, Lusk CP, Blobel G (2006). Karyopherin-mediated import of integral inner nuclear membrane proteins. Nature 442, 1003–1007.
Koning AJ, Lum PY, Williams JM, Wright R (1993). DiOC6 staining reveals organelle structure and dynamics in living yeast cells. Cell Motil Cytoskeleton 25, 111–128.
Kumar S, Stecher G, Tamura K (2016). MEGA7: Molecular Evolutionary Genetics Analysis version 7.0 for bigger datasets. Mol Biol Evol 33, 1870–1874.
Liu HL, Osmani AH, Ukil L, Son S, Markossian S, Shen KF, Govindaraghavan M, Varadaraj A, Hashmi SB, De Souza CP, Osmani SA (2010). Single-step affinity purification for fungal proteomics. Eukaryot Cell 9, 831–833.
Liu HL, De Souza CP, Osmani AH, Osmani SA (2009). The three fungal transmembrane nuclear pore complex proteins of Aspergillus nidulans are dispensable in the presence of an intact An-Nup84–120 complex. Mol Biol Cell 20, 616–630.
Lusk CP, Blobel G, King MC (2007). Highway to the inner nuclear membrane: rules for the road. Nat Rev Mol Cell Biol 8, 414–420.
Ma Y, Cai S, Lv Q, Jiang Q, Zhang Q, Sodmergen, Zhai Z, Zhang C (2007). Lamin B receptor plays a role in stimulating nuclear envelope production and targeting membrane vesicles to chromatin during nuclear envelope assembly through direct interaction with importin beta. J Cell Sci 120, 520–530.
Malhas A, Goulbourne C, Vaux DJ (2011). The nucleoplasmic reticulum: form and function. Trends Cell Biol 21, 362–373.
Markina-Inarrairaegui A, Etxebeste O, Herrero-Garcia E, Araujo-Bazan L, Fernandez-Martinez J, Flores JA, Osmani SA, Espeso EA (2011). Nuclear transporters in a multinucleated organism: functional and localization analyses in Aspergillus nidulans. Mol Biol Cell 22, 3874–3886.
Masuda M, Oshima A, Noguchi T, Kagiwada S (2016). Induction of intranuclear membranes by overproduction of Opi1p and Scs2p, regulators for yeast phospholipid biosynthesis, suggests a mechanism for Opi1p nuclear translocation. J Biochem 159, 351–361.
Meinema AC, Laba JK, Hapsari RA, Otten R, Mulder FA, Kralt A, van den Bogaart G, Lusk CP, Poolman B, Veenhoff LM (2011). Long unfolded linkers facilitate membrane protein import through the nuclear pore complex. Science 333, 90–93.
Meseroll RA, Cohen-Fix O (2016). The malleable nature of the budding yeast nuclear envelope: flares, fusion, and fenestrations. J Cell Physiol 231, 2353–2360.
Nayak T, Szewczyk E, Oakley CE, Osmani A, Ukil L, Murray SL, Hynes MJ, Osmani SA, Oakley BR (2006). A versatile and efficient gene-targeting system for Aspergillus nidulans. Genetics 172, 1557–1566.
Nousiainen HO, Kestila M, Pakkasjarvi N, Honkala H, Kuure S, Tallila J, Vuopala K, Ignatius J, Herva R, Peltonen L (2008). Mutations in mRNA export mediator GLE1 result in a fetal motoneuron disease. Nat Genet 40, 155–157.
Osmani AH, Davies J, Liu HL, Nile A, Osmani SA (2006a). Systematic deletion and mitotic localization of the nuclear pore complex proteins of Aspergillus nidulans. Mol Biol Cell 17, 4946–4961.
Osmani AH, Oakley BR, Osmani SA (2006b). Identification and analysis of essential Aspergillus nidulans genes using the heterokaryon rescue technique. Nat Protoc 1, 2517–2526.
Pontecorvo G, Roper JA, Hemmons LM, Macdonald KD, Bufton AW (1953). The genetics of Aspergillus nidulans. Adv Genet 5, 141–238.
Prunuske AJ, Ullman KS (2006). The nuclear envelope: form and reformation. Curr Opin Cell Biol 18, 108–116.
Ralle T, Grund C, Franke WW, Stick R (2004). Intranuclear membrane structure formations by CaaX-containing nuclear proteins. J Cell Sci 117, 6095–6104.
Rayala HJ, Kendirgi F, Barry DM, Majerus PW, Wente SR (2004). The mRNA export factor human Gle1 interacts with the nuclear pore complex protein Nup155. Mol Cell Proteomics 3, 145–155.
Saunders DG, Dagdas YF, Talbot NJ (2010). Spatial uncoupling of mitosis and cytokinesis during appressorium-mediated plant infection by the rice blast fungus Magnaporthe oryzae. Plant Cell 22, 2417–2428.
Suelmann R, Sievers N, Fischer R (1997). Nuclear traffic in fungal hyphae: in vivo study of nuclear migration and positioning in Aspergillus nidulans. Mol Microbiol 25, 757–769.
Szewczyk E, Nayak T, Oakley CE, Edgerton H, Xiong Y, Taheri-Talesh N, Osmani SA, Oakley BR (2006). Fusion PCR and gene targeting in Aspergillus nidulans. Nat Protoc 1, 3111–3120.
Talamas JA, Hetzer MW (2011). POM121 and Sun1 play a role in early steps of interphase NPC assembly. J Cell Biol 194, 27–37.
Ukil L, De Souza CP, Liu HL, Osmani SA (2009). Nucleolar separation from chromosomes during Aspergillus nidulans mitosis can occur without spindle forces. Mol Biol Cell 20, 2132–2145.
Vukovic LD, Jevtic P, Edens LJ, Levy DL (2016). New insights into mechanisms and functions of nuclear size regulation. Int Rev Cell Mol Biol 322, 1–59.
Walters AD, Bommakanti A, Cohen-Fix O (2012). Shaping the nucleus: factors and forces. J Cell Biochem 113, 2813–2821.

Waring RB, May GS, Morris NR (1989). Characterization of an inducible expression system in Aspergillus nidulans using alcA and tubulin-coding genes. Gene 79, 119–130.
Webster M, Witkin KL, Cohen-Fix O (2009). Sizing up the nucleus: nuclear shape, size and nuclear-envelope assembly. J Cell Sci 122, 1477–1486.
Wigge PA, Kilmartin JV (2001). The Ndc80p complex from Saccharomyces cerevisiae contains conserved centromere components and has a function in chromosome segregation. J Cell Biol 152, 349–360.
Witkin KL, Chong Y, Shao S, Webster MT, Lahiri S, Walters AD, Lee B, Koh JL, Prinz WA, Andrews BJ, Cohen-Fix O (2012). The budding yeast nuclear envelope adjacent to the nucleolus serves as a membrane sink during mitotic delay. Curr Biol 22, 1128–1133.
Wolfner MF, Wilson KL (2001). The nuclear envelope: emerging roles in development and disease. Cell Mol Life Sci 58, 1737–1740.
Worman HJ (2004). Nuclear envelope proteins and human disease. Symp Soc Exp Biol 41–55.
Worman HJ, Ostlund C, Wang Y (2010). Diseases of the nuclear envelope. Cold Spring Harb Perspect Biol 2, a000760.
Wright R, Basson M, D'Ari L, Rine J (1988). Increased amounts of HMG-CoA reductase induce "karmellae": a proliferation of stacked membrane pairs surrounding the yeast nucleus. J Cell Biol 107, 101–114.
Yang L, Ukil L, Osmani A, Nahm F, Davies J, De Souza CP, Dou X, Perez-Balaguer A, Osmani SA (2004). Rapid production of gene replacement constructs and generation of a green fluorescent protein-tagged centromeric marker in Aspergillus nidulans. Eukaryot Cell 3, 1359–1362.
Zink D, Fischer AH, Nickerson JA (2004). Nuclear structure in cancer cells. Nat Rev Cancer 4, 677–687.